JP2.16 DERIVATION AND TESTS OF THE GCSS ANALYTIC LONGWAVE RADIATION FORMULA

Kurt E. Kotenberg[1] Norman B. Wood[2] Vincent E. Larson[1*]
[1]Atmospheric Science Group, Dept. of Mathematical Sciences, University of Wisconsin — Milwaukee.
[2] Dept. of Atmospheric Science, Colorado State University, Fort Collins, CO.

1. ABSTRACT

Many GCSS intercomparisons of boundary layer clouds have used a convenient but idealized longwave radiation formula for clouds in their large-eddy simulations (LES). Under what conditions is this formula justified? Can it be extended to mid-level layer clouds?

This paper first derives the GCSS formula using an alternative method to effective emissivity. A key simplifying assumption is that the cloud is isothermal in the vertical and horizontal. However, this assumption does not turn out to be overly restrictive in practice. Then the GCSS formula is compared with a detailed numerical code, BugsRad. Sensitivity studies are performed in which cloud properties, cloud altitude, and thermodynamic profiles are modified. Our focus is primarily on mid-level, altostratocumulus layers.

Our results show that the GCSS formula can be successfully extended to liquid (ice-free), mid-level clouds. The GCSS formula produces remarkably accurate radiative profiles if the parameters are adjusted on a case-by-case basis. However, the formula needs to be calibrated using a more general radiative transfer code.

2. INTRODUCTION: WHY IS AN ANALYTIC RADIATIVE TRANSFER FORMULA USEFUL FOR CLOUD SIMULATIONS?

Large-eddy simulation (LES) is a useful technique for modeling thin cloud layers. Overcast cloud layers often contain turbulence that is driven by longwave radiative transfer. LES models often use *analytic* within-cloud longwave radiative transfer formulas for three reasons. First, an analytic formula is easy to implement in a model. This aids model intercomparisons in particular, because all participants can easily implement the same radiative formula. Second, LES usually last six hours or less, a period too short to heat or cool clear air significantly, thereby vitiating the advantage of accurate multi-band radiative calculations for gaseous absorption. Third, an analytic longwave formula is computationally inexpensive. This is advantageous because considerable expense is associated with both LES and numerical radiation calculations. LES is expensive because it requires a small grid size (often tens of meters) and numerous grid columns (often 100 in each horizontal direction). Numerical radiation calculations are expensive in part because longwave radiation can be exchanged over many kilometers in the vertical, from far below cloud base to far above cloud top.

An analytic longwave formula has been used with success in stratocumulus intercomparisons by Global Energy and Water Cycle Experiment (GEWEX) Cloud System Study (GCSS) (Bretherton and Co-Authors 1999; Bretherton et al. 1999; Duynkerke et al. 1999; Stevens and Co-Authors 2001; Duynkerke and Co-Authors 2004; Stevens and Co-Authors 2005). This formula for radiative flux is a simple exponential of liquid water path (LWP). Although this formula can be seen to be a special case of the effective emissivity model (Cox 1976; Stephens 1978, 1984; MacVean 1993), the formula's derivation is apparently not widely known in the LES intercomparison community, because none of the above intercomparisons references a derivation. One goal of this paper is to provide an alternative derivation to the effective emissivity approach, thereby exposing the assumptions under which it is valid. Another goal is to test the formula's applicability to thin, overcast, liquid, mid-level clouds. Although these clouds are structurally similar to boundary layer stratocumulus, they reside farther above ground and hence have larger cloud base heating rates. The GCSS formula has already been applied to a mid-level cloud by Larson et al. (2006).

The outline of this paper is as follows. In section 2, we derive the GCSS radiative transfer formula. In section 3, we compare this analytic formula to a sophisticated two-stream numerical radiative transfer model, BugsRad. As a test case, we use an altostratocumulus (i.e. overcast altocumulus, see Larson et al. (2006)) cloud that was observed by Fleishauer et al. (2002). We perform various sensitivity studies to test the generality of the analytic formula. Additionally, we test the formula on a boundary layer stratocumulus case. In section 4, we present conclusions.

3. DERIVATION OF THE RADIATIVE TRANSFER APPROXIMATION

In this section, we derive the longwave formula that has been used in GCSS intercomparisons. We follow the methodology of Goody (1995) rather than the effective emissivity approach of Cox (1976), Stephens (1978), and Stephens (1984). To increase computational speed, the formula retains only a single

[*]*Corresponding author address:* Vincent E. Larson, Department of Mathematical Sciences, University of Wisconsin – Milwaukee, P. O. Box 413, Milwaukee, WI 53201-0413, vlarson at uwm dot edu, http://www.uwm.edu/∼vlarson .

wavenumber band, that is, the formula is a grey model. We use the method of moments to average over the angular distribution of radiation, leaving a two-stream model with upward and downward streams.

The modeled cloud is idealized. Its geometry is a horizontally infinite uniform slab of finite thickness. We assume that everywhere within cloud there is constant asymmetry parameter, single-scattering albedo, mass extinction cross section, and temperature. The within-cloud radiation is assumed to be forced by constant downwelling radiation from above and constant upwelling radiation from below.

Given these assumptions, the governing equation for the net upwards longwave radiative flux, F, can be written (Goody 1995, p. 118):

$$\frac{d^2F}{d\tau^2} = \alpha^2 F \qquad \alpha^2 = 3(1-\omega)(1-\omega g). \tag{1}$$

Here F is the upwelling flux minus the downwelling flux (with units of W m^{-2}), ω is the single-scattering albedo, and g is the asymmetry factor. The single-scattering albedo, ω, is the probability that a droplet scatters rather than absorbs, where $\omega = 1$ represents complete scattering and $\omega = 0$ represents complete absorption. The asymmetry factor, g, indicates the degree of forward or backward scattering, with $g = 1$ for complete forward scattering and $g = 0$ for isotropic scattering. The optical depth, τ, ranges from zero at the top of the cloud to a positive number at cloud base. It is related to the liquid water path from cloud top to altitude z, $LWP(z)$, by

$$\tau(z) = \frac{e}{m} LWP(z). \tag{2}$$

Here e is the extinction cross-section with units of area, and m is the mass of each droplet. We define $LWP(z)$ as the integral:

$$LWP(z) = \int_{z'=z}^{z'=\infty} \rho(z')\, r_c(z')\; dz', \tag{3}$$

where ρ is the density of dry air and r_c is cloud water mixing ratio.

To solve (1), boundary conditions are needed at cloud top and base. Just above cloud top, we set the downwelling radiance to $B_t = (\sigma/\pi)T_t^4$. Here σ is the Stefan-Boltzmann constant, and T_t represents an effective radiative temperature of air above the cloud (not the cloud-top temperature itself). Then we derive the following "mixed" boundary condition (see Goody 1995, p. 114-115):

$$\left.\frac{dF}{d\tau}\right|_{\tau=0} = 4\pi(1-\omega)\left[\frac{F|_{\tau=0}}{2\pi} - (B - B_t)\right]. \tag{4}$$

Here $B = (\sigma/\pi)T^4$ is the emitted radiance from the cloud, assumed to have an effective temperature T. Also, $F|_{\tau=0}$ is the *net* flux at cloud top (upwelling minus downwelling), which is unknown because only the downwelling component is specified. Likewise, at cloud base, we set the upwelling radiance to B_b:

$$\left.\frac{dF}{d\tau}\right|_{\tau=\tau_b} = 4\pi(1-\omega)\left[(B_b - B) - \frac{F|_{\tau=\tau_b}}{2\pi}\right]. \tag{5}$$

By inspection, we see that (1) has a solution of the form

$$F = Le^{\alpha\tau} + Me^{-\alpha\tau}. \tag{6}$$

The constants L and M are found by substituting (6) into the boundary conditions (4) and (5). We find

$$\begin{aligned} L &= \gamma\left[(B - B_t)c_1 e^{-\alpha\tau_b} + (B_b - B)c_2\right] \\ M &= \gamma\left[(B - B_t)c_2 e^{\alpha\tau_b} + (B_b - B)c_1\right], \end{aligned} \tag{7}$$

where

$$\gamma = \frac{-4\pi(1-\omega)}{c_1^2 e^{-\alpha\tau_b} - c_2^2 e^{\alpha\tau_b}} \tag{8}$$

and

$$c_1 = \alpha - 2(1-\omega) \qquad c_2 = \alpha + 2(1-\omega). \tag{9}$$

Here τ_b is the optical depth at cloud base.

In a LES, the cloud field is affected directly not by the radiative flux, but rather the heating rate, defined as:

$$\left(\frac{\partial T}{\partial t}\right)_{\mathrm{Rad}} = -\frac{1}{\rho c_p}\frac{\partial F}{\partial z}, \tag{10}$$

where c_p is the specific heat of air at constant pressure. To compute $\partial F/\partial z$, we use the chain rule:

$$\frac{\partial F}{\partial z} = \frac{\partial F}{\partial \tau}\frac{\partial \tau}{\partial z} = -\frac{e}{m}\rho r_c \alpha\left(Le^{\alpha\tau} - Me^{-\alpha\tau}\right). \tag{11}$$

In GCSS intercomparisons, the following notation has often been used:

$$F_0 \equiv M \qquad F_1 \equiv Le^{\alpha\tau_b} \qquad \kappa \equiv \alpha\frac{e}{m}. \tag{12}$$

Substituting (11) into (10) and re-writing in the GCSS notation (12), we have finally

$$\begin{aligned} \left(\frac{\partial T}{\partial t}\right)_{\mathrm{Rad}} = -\frac{1}{\rho c_p}\kappa\rho r_c \Big[& F_0 e^{-\kappa LWP(z)} \\ & - F_1 e^{-\kappa[LWP_b - LWP(z)]}\Big]. \end{aligned} \tag{13}$$

The F_0 term represents cloud-top radiative cooling; the F_1 term represents cloud-base radiative heating. If the cloud is thick enough that the F_0 and F_1 terms do not overlap (as in Fig. 4 below) then we may interpret F_0 as the net radiative flux at cloud top, F_1 as the net radiative flux at cloud base, and κ as a factor that represents absorptivity. A key to obtaining this simple exponential form is to assume that the cloud layer is isothermal. In this expression, the ρs may be cancelled from the numerator and denominator of the prefactor; they have been written explicitly to preserve the combination ρc_p.

The approximation (13) can be shown to be equivalent to the "effective emissivity" model (Cox 1976; Stephens 1978, 1984) when the within-cloud temperature is constant and the absorption coefficients are assumed equal for upward and downward radiation streams. Stephens (1978) chooses the upward and downward absorption coefficients to be 130 m^2 kg^{-1} and 158 m^2 kg^{-1}, respectively, whereas we use $\kappa = 119$ m^2 kg^{-1} in the calculations below. The value $\kappa = 130$ m^2 kg^{-1} has been used in past intercomparisons (Duynkerke et al. 1999; Duynkerke and Co-Authors 2004). To what values of effective radius r_e do these κ values correspond? Although there is no unique relationship between κ and r_e, under typical conditions $\kappa \propto 1/r_e$ to a very crude approximation. Example calculations using the BugsRad radiative transfer model show that $\kappa = 160$ corresponds roughly to $r_e = 5\mu$m and $\kappa = 105$ to $r_e = 12.5\mu$m (Table 1). This may be useful for modelers who wish to understand how effective radius affects cooling rates and turbulence levels in layer clouds.

The formula (13) only accounts for radiative heating or cooling within cloud. To represent radiative cooling of air above cloud top ($z > z_t$), Stevens and Co-Authors (2005) augment (13), leading to the combined formula

$$\begin{aligned}\left(\frac{\partial T}{\partial t}\right)_{\mathrm{Rad}} = & -\frac{1}{\rho c_p}\kappa\rho r_c\Big[F_0 e^{-\kappa LWP(z)} \\ & -F_1 e^{-\kappa[LWP_b - LWP(z)]}\Big] \\ & -D(A_z/3)H(z-z_t)\Big[(z-z_t)^{1/3} \\ & +z_0(z-z_t)^{-2/3}\Big]. \qquad (14)\end{aligned}$$

The F_0 and F_1 terms are meant to be applied only in cloud. In the last two terms, D is the large-scale horizontal divergence rate with units of inverse time, $A_z = 1$ K m$^{-1/3}$ is a constant that yields the correct units, z_t is the altitude of cloud top, $z_0 = 840$ m is a constant of the order of the turbulent layer thickness, and H is the Heaviside step function, which restricts the clear-air cooling to above-cloud areas ($H(z-z_t) = 0$ for $z < z_t$ and $H(z-z_t) = 1$ for $z > z_t$). Since subsidence is known imprecisely, we treat D as a tuning parameter. We neglect heating and cooling below cloud base. One drawback of this formula is that the $(z-z_t)^{-2/3}$ factor becomes arbitrarily large as z approaches z_t from above. This renders the results sensitive to grid spacing.

4. WHEN IS THE GCSS RADIATIVE APPROXIMATION ACCURATE?

We now compare the simple approximation (14) with calculations by a sophisticated numerical radiative transfer model, BugsRad (Stephens et al. 2001, 2004). BugsRad is a two-stream model that computes hydrometeor scattering and absorption, molecular scattering, and gaseous absorption. Gaseous absorption is computed using the correlated-k distribution method (Fu and Liou 1992). Cloud droplet optical properties, including extinction cross section e, are computed using anomalous diffraction theory (e.g. Ackerman and Stephens 1987). Cloud droplet size distributions are treated as modified gamma distributions with dispersion of 2.0 (Stephens et al. 1990). Cloud droplets are assumed to have a fixed effective radius in the vertical and horizontal, which we set to 10 microns unless stated otherwise. At scales of tens of meters, three-dimensional radiative effects, which are ignored by BugsRad, may be significant. However, 3D effects are likely to be less important for longwave than for shortwave radiation. For our cases, we used a fine within-cloud vertical grid spacing of about 8 m.

In all our comparisons with BugsRad, the analytic formula (14) will use $g = 0.83$ and $\omega = 0.694$. Additionally, we keep constant the standard-case value of κ (119 m^2 kg^{-1}) in all cases except those in which we change effective radius.

To make contact with prior work on the analytic formula (14), we first compare it to BugsRad calculations for a boundary layer stratocumulus cloud (Stevens and Co-Authors 2005) that was observed during Research Flight 01 of the second Dynamics and Chemistry of Marine Stratocumulus (DYCOMS-II) field experiment (see Fig. 1). The input fields are the initial profiles (Stevens and Co-Authors 2005) from the GCSS LES intercomparison of this case. Stevens and Co-Authors (2005) computed radiative transfer through this cloud using the numerical model of Fu and Liou (1993) and the analytic formula (14) with parameter values $F_0 = 70$ W m^{-2}, $F_1 = 22$ W m^{-2}, and $\kappa = 85$ m^2 kg^{-1}. Our calculated radiative profiles resemble theirs, and our best-fit values to BugsRad are similar: $F_0 = 62$ W m^{-2}, $F_1 = 17.7$ W m^{-2}, and $\kappa = 100$ m^2 kg^{-1}. However, when we use $\kappa = 119$ m^2 kg^{-1}, as in Fig. 1, the fit is still adequate. The best-fit value of κ increases somewhat with increasing resolution because the peak in cloud-top cooling is narrow.

Fig. 1 is divided into five panels. Panel (a) shows the heating rate, as calculated by both BugsRad (solid line) and (14) (dot-dashed line). The two calculations agree well. At cloud top there is strong cooling, and at cloud base there is slight heating. The cloud top cools because it radiates strongly upward and receives little compensating downwelling radiation from above. The cloud base heats because it emits less radiant energy than it receives from the warmer ocean surface below. The cooling minimum produced by BugsRad just above cloud top is due to a thin humid layer there (above top of plot). Panel (b) shows that analytic and BugsRad calculations also agree well for net radiative flux (upwelling minus downwelling). Panels (c), (d), and (e) display the input profiles of cloud water mixing ratio, water vapor specific humidity, and temperature.

Next we examine an overcast altostratocumulus (ASc) layer that was observed on 11 Nov 1999 during the Complex Layered-cloud Experiment 5 (CLEX-5, Fleishauer et al. (2002)). This cloud resided roughly 5.6

km above mean sea level and decayed with time. Its cloud-top cloud water mixing ratio evolved from an initial value of $r_c \cong 0.43$ g kg^{-1} to zero (Larson et al. 2001; Fleishauer et al. 2002). Because the analytic radiative formula (14) is intended for use in LES models, we input horizontally averaged profiles generated by LES into the radiative scheme. Above and below the LES model domain, we merge a nearby radiosonde profile.

Our standard altostratocumulus (ASc) case is displayed in Fig. 2. The input r_c profile has already decayed, leaving $r_c \sim 0.2$ g kg^{-1} at cloud top. We use the best-fit values $F_0 = 96.2$ W m^{-2}, $F_1 = 61.2$ W m^{-2}, and $\kappa = 119$ m^2 kg^{-1}. Compared to the aforementioned stratocumulus layer, our ASc cloud has smaller r_c (and higher altitude) and therefore smaller cloud-top cooling. However, the ASc cloud base heating is substantially larger. This is because the temperature difference between cloud base and ground is much larger for ASc than for stratocumulus.

We now perform sensitivity studies in order to test the range of validity of the analytic formula. To isolate effects, we change only one profile (e.g. cloud water) at a time. In some cases this procedure leads to incompatible combinations of profiles (e.g. the presence of liquid in subsaturated air). However, this is acceptable, since our purpose is to isolate the influence of individual parameters on a radiation formula, not model the time evolution of cloud fields.

A key assumption of our analytic formula (14) is that the cloud is isothermal. How much can the temperature vary between cloud top and cloud base before the analytic formula breaks down? To test this, we increase the cloud base temperature until it is 20 K warmer than cloud top (see Fig. 3). Even with this enormous variation in temperature, the analytic formula is still moderately accurate. However, the analytic flux profile does not vary enough from cloud top to base, and adjusting the parameters does not improve the overall shape.

Next we increase cloud water mixing ratio, r_c (see Fig. 4). The analytic formula, with little change in F_0 and F_1 from the standard case, still matches BugsRad. Cloud-top cooling is increased (to $\cong$13 K hr^{-1}) because r_c has increased. If we decrease r_c (Fig. 5) from the standard profile, then our analytic formula again matches BugsRad, with a somewhat larger change in F_0 and F_1. Because r_c is small, the cloud-top cooling becomes small ($\cong$1 K hr^{-1}). In addition, the cloud base heating vanishes, despite the large temperature difference between ground and cloud base. This is because r_c is especially low near cloud base, leading to little absorption there. The above-cloud cooling profile in (14) no longer matches BugsRad well.

Next we vary cloud altitude. We first decrease cloud-top pressure to 300 mb (Fig. 6) and later increase cloud-top pressure to 800 mb, moving the cloud near the planetary boundary layer (Fig. 7). In either case, the cloud-top cooling deviates little from the standard case, but the cloud-base heating changes considerably. When we increase cloud altitude, the temperature difference between ground and cloud base increases, leading to more cloud-base heating and necessitating a larger value of F_1 (102 W m^{-2}) (Fig. 6). When we decrease cloud altitude, the cloud-base heating nearly vanishes and consequently F_1 decreases to 14.9 W m^{-2} (Fig. 7).

Next we dry the air above cloud by multiplying the vapor mixing ratio there by 0.4 (not shown). This increases cloud-top cooling and requires a slight increase in F_0 to 111 W m^{-2}. If we multiply the vapor mixing ratio *below* cloud by 0.4, then cloud-base heating and $F_1 = 69.9$ W m^{-2} increase slightly (not shown). In both cases, we obtain a good fit.

Finally we vary the droplet effective radius, defined as $r_e \equiv \overline{r^3}/\overline{r^2}$, while holding r_c fixed. If we decrease r_e to 5 microns (not shown), then cloud-top cooling and cloud-base heating increase slightly, and the heating and cooling rates increase, as when r_c is increased. This is because the total cross-sectional area of the droplets has increased, leading to greater cloud optical thickness. In this case, $\kappa(= 172$ m^2 kg$^{-1})$ must be increased substantially to match BugsRad. If we increase r_e to 15 microns (not shown), then the opposite effects occur. In both cases, a good fit is obtained.

The best-fit values of our parameters F_0, F_1, and D are summarized in Table 2. This illustrates the variation in parameter values over a wide range of conditions. The heating rate errors for our analytical formula are listed in Table 3. In all cases, the root-mean-square heating error is less than 0.33 K hr^{-1}.

5. SUMMARY OF RESULTS AND CONCLUSIONS

Our first contribution is to provide an alternative derivation of an analytic within-cloud radiation formula (14) that has been widely used in GCSS and other intercomparisons of boundary layer clouds (e.g. Bretherton and Co-Authors 1999; Bretherton et al. 1999; Duynkerke et al. 1999; Stevens and Co-Authors 2001; Duynkerke and Co-Authors 2004; Stevens and Co-Authors 2005). The formula is applicable to liquid-only layer clouds. A key assumption is that the cloud layer has constant temperature in the vertical, leading to a simple exponential formula. In practice, however, even large temperature differentials (20 K) do not lead to unacceptable errors (see Fig. 3).

The analytic formula (14) contains four main adjustable parameters: F_0 controls cloud-top cooling, F_1 controls cloud-base heating, κ controls cloud absorptivity, and D controls above-cloud cooling. When these are optimized for individual cases, the formula can yield remarkably accurate fluxes and heating rates. However, these parameter values must be obtained on a case-by-case basis by comparing, for instance, with a sophisticated numerical code such as BugsRad. Although for most cases we have been able to set $\kappa = 119$ m^2 kg^{-1}, F_0 and F_1 must change as the cloud base and top temperatures change.

On the other hand, if the cloud water in a LES were to change *between grid columns or during runtime* (e.g.

Stevens and Co-Authors 2005; Larson et al. 2006), the best-fit parameter values would not change markedly (see Figs. 4 and 5). This allows us to use one set of parameter values for each grid column and time step throughout an LES. Then, to account for the effect of horizontal liquid fluctuations on radiative fluxes, a LES can simulate the horizontal fluctuations in liquid and apply the analytic radiative formula to each column.

What is the value of an analytic formula if we must first run a numerical radiation code to calibrate it? The first benefit is that an analytic formula reduces computational cost during runtime. The second benefit is that the numerical radiation code need only be run in standalone mode, thereby avoiding the effort required to implement the radiation code in a LES model. Recall that a LES of layer clouds simulates only a thin slab of the atmosphere. If a numerical radiation code is implemented in the LES, then either radiative fluxes must be specified at upper and lower boundaries, which is usually obtained from a separate standalone radiation calculation, or else the radiative fluxes must be computed during runtime far above and/or below the LES boundaries, thereby requiring more computational time.

Finally, we have shown that the GCSS radiation formula, which has been applied with success to boundary layer stratocumulus, can also be applied to mid-level clouds, if the parameter values are adjusted. In particular, F_1 must be increased in order to account for increased cloud-base heating.

We hope that documenting these tests of the GCSS radiation formula provides a useful service to the community. The authors freely provide the BugsRad code to those who desire to customize the GCSS formula for their cloud cases.

Acknowledgements V. E. Larson and K. E. Kotenberg are grateful for financial support provided by Grant ATM-0239982 from the National Science Foundation, and by subaward G-7424-1 from the DoD Center for Geosciences/Atmospheric Research at Colorado State University via Cooperative Agreement DAAD19-02-2-0005 with the Army Research Laboratory. N. Wood acknowledges support from the U. S. Department of Energy Atmospheric Radiation Measurement program under grant DE-FG03-94ER61748.

References

Ackerman, S. A. and G. L. Stephens, 1987: The absorption of solar radiation by cloud droplets: An application of anomalous diffraction theory. *J. Atmos. Sci.*, **44**, 1475–1588.

Bretherton, C. S. and Co-Authors, 1999: An intercomparison of radiatively driven entrainment and turbulence in a smoke cloud, as simulated by different numerical models. *Quart. J. Roy. Meteor. Soc.*, **125**, 391–423.

Bretherton, C. S., S. K. Krueger, M. C. Wyant, P. Bechtold, E. van Meijgaard, B. Stevens, and J. Teixeira, 1999: A GCSS boundary-layer cloud model intercomparison study of the first ASTEX Lagrangian experiment. *Bound.-Layer Meteor.*, **93**, 341–380.

Cox, S. K., 1976: Observations of cloud infrared effective emissivity. *J. Atmos. Sci.*, **33**, 287–289.

Duynkerke, P. G. and Co-Authors, 2004: Observations and numerical simulations of the diurnal cycle of the EUROCS stratocumulus case. *Quart. J. Roy. Meteor. Soc.*, **130**, 3269–3296.

Duynkerke, P. G., P. J. Jonker, A. Chlond, M. C. Van Zanten, J. Cuxart, P. Clark, E. Sanchez, G. Martin, G. Lenderink, and J. Teixeira, 1999: Intercomparison of three- and one-dimensional model simulations and aircraft observations of stratocumulus. *Bound.-Layer Meteor.*, **92**, 453–487.

Fleishauer, R. P., V. E. Larson, and T. H. Vonder Haar, 2002: Observed microphysical structure of midlevel, mixed-phase clouds. *J. Atmos. Sci.*, **59**, 1779–1804.

Fu, Q. and K.-N. Liou, 1992: On the correlated k-distribution method for radiative transfer in nonhomogeneous atmospheres. *J. Atmos. Sci.*, **49**, 2139–2156.

Fu, Q. and K.-N. Liou, 1993: Parameterization of the radiative properties of cirrus clouds. *J. Atmos. Sci.*, **50**, 2008–2025.

Goody, R. M., 1995: *Principles of Atmospheric Physics and Chemistry*. Oxford University Press, 324 pp.

Larson, V. E., R. P. Fleishauer, J. A. Kankiewicz, D. L. Reinke, and T. H. Vonder Haar, 2001: The death of an altocumulus cloud. *Geophys. Res. Lett.*, **28**, 2609–2612.

Larson, V. E., A. J. Smith, M. J. Falk, K. E. Kotenberg, and J.-C. Golaz, 2006: What determines altocumulus dissipation time? Submitted to *J. Geophys. Res.*

MacVean, M. K., 1993: A numerical investigation of the criterion for cloud-top entrainment instability. *J. Atmos. Sci.*, **50**, 2481–2495.

Stephens, G. L., 1978: Radiation profiles in extended water clouds. II: Parameterization schemes. *J. Atmos. Sci.*, **35**, 2123–2132.

Stephens, G. L., 1984: The parameterization of radiation for numerical weather prediction and climate models. *Mon. Wea. Rev.*, **112**, 826–867.

Stephens, G. L., S.-C. Tsay, J. P. W. Stackhouse, and P. J. Flatau, 1990: The relevance of the microphysical and radiative properties of cirrus clouds to climate and climatic feedback. *J. Atmos. Sci.*, **47**, 1742–1753.

Stephens, G. L., P. M. Gabriel, and P. T. Partain, 2001: Parameterization of atmospheric radiative transfer. Part I: Validity of simple models. *J. Atmos. Sci.*, **58**, 3391–3409.

Stephens, G. L., N. Wood, and P. Gabriel, 2004: An assessment of the parameterization of subgrid-scale cloud effects on radiative transfer. Part I: Vertical overlap. *J. Atmos. Sci.*, **61**, 715–732.

Stevens, B. and Co-Authors, 2001: Simulations of trade wind cumuli under a strong inversion. *J. Atmos. Sci.*, **58**, 1870–1891.

Stevens, B. and Co-Authors, 2005: Evaluation of large-eddy simulations via observations of nocturnal marine stratocumulus. *Mon. Wea. Rev.*, **133**, 1443–1462.

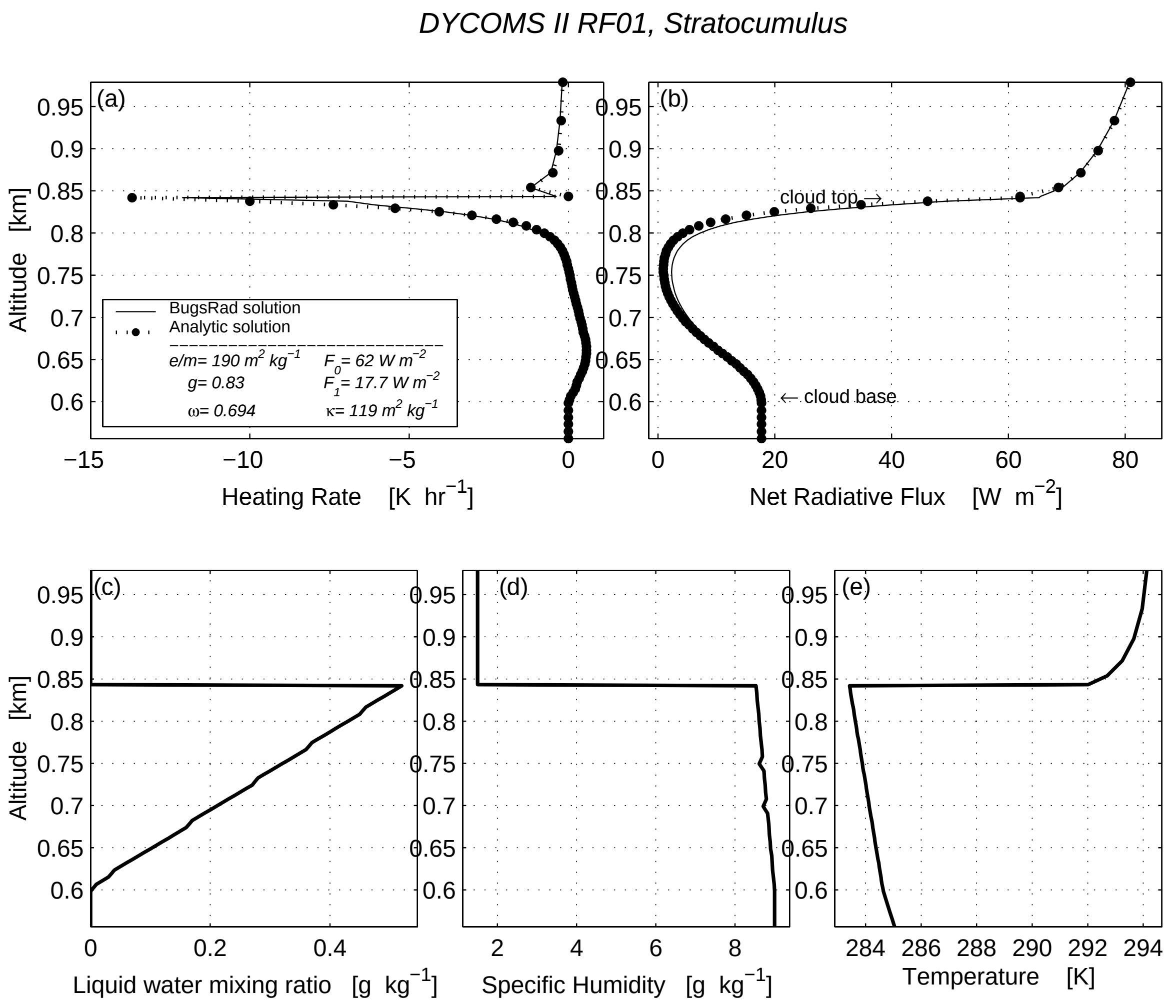

Figure 1: Radiative and thermodynamic profiles for the DYCOMS-II RF01 boundary layer stratocumulus cloud. Panel (a) shows longwave radiative heating rate. Panel (b) shows net longwave radiative flux (upwelling stream minus downwelling stream). In these panels, a solid line denotes the solution obtained by a numerical radiation code, BugsRad; the dashed-dotted line denotes the analytic solution corresponding to (14). Panels (c), (d), and (e) show, respectively, the profiles of cloud water mixing ratio r_c, specific humidity, and temperature. There is strong cloud-top radiative cooling and minimal cloud-base radiative heating.

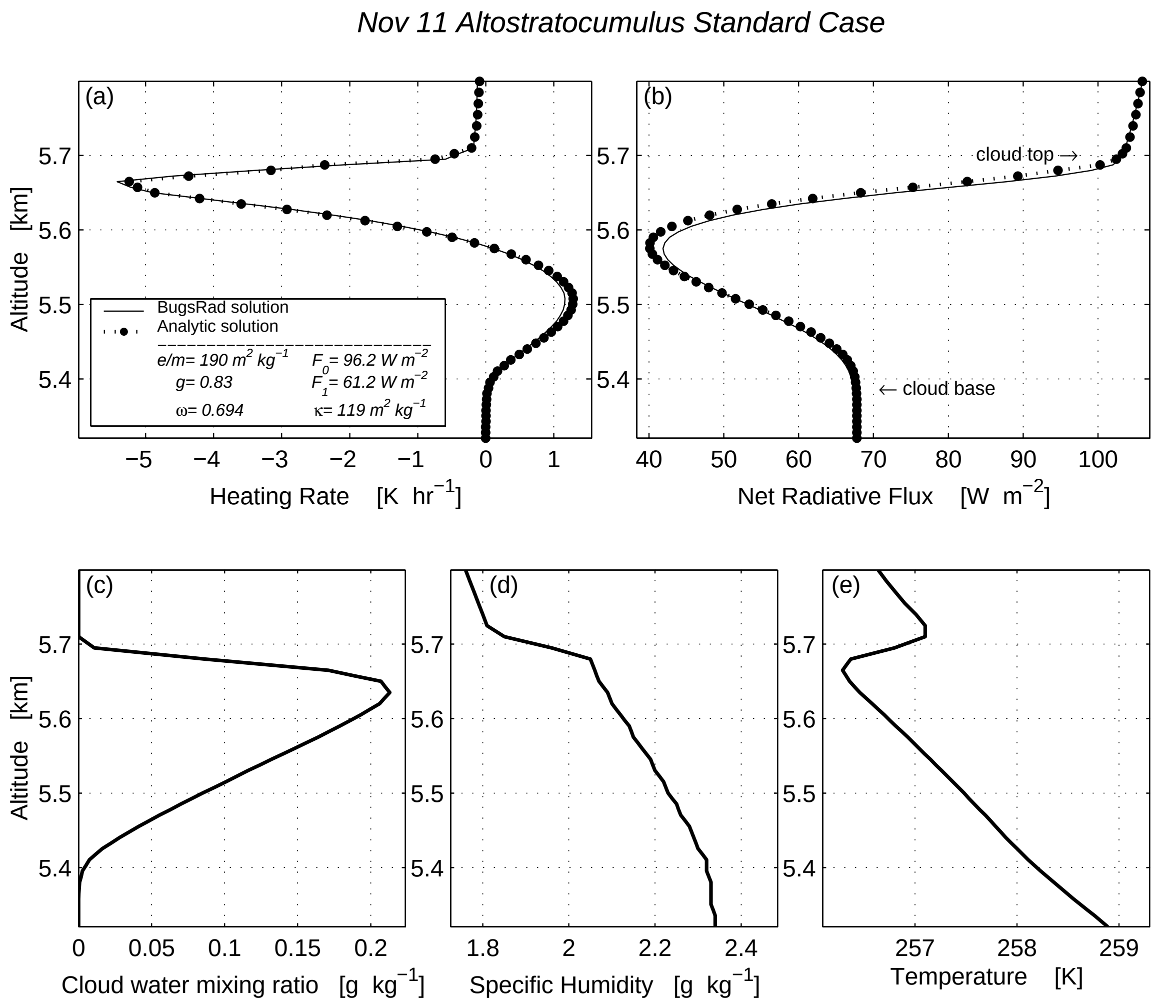

Figure 2: Radiative and thermodynamic profiles for the standard Nov 11 altostratocumulus cloud. Panels (a) and (b) show, respectively, longwave radiative heating rate and net flux due to BugsRad (solid) and the analytic formula (dashed-dot). Panels (c), (d), and (e) show, respectively, horizontally averaged profiles of cloud water mixing ratio r_c, specific humidity, and temperature obtained from a LES. Cloud-base heating is strong because the temperature difference between cloud base and ground is large.

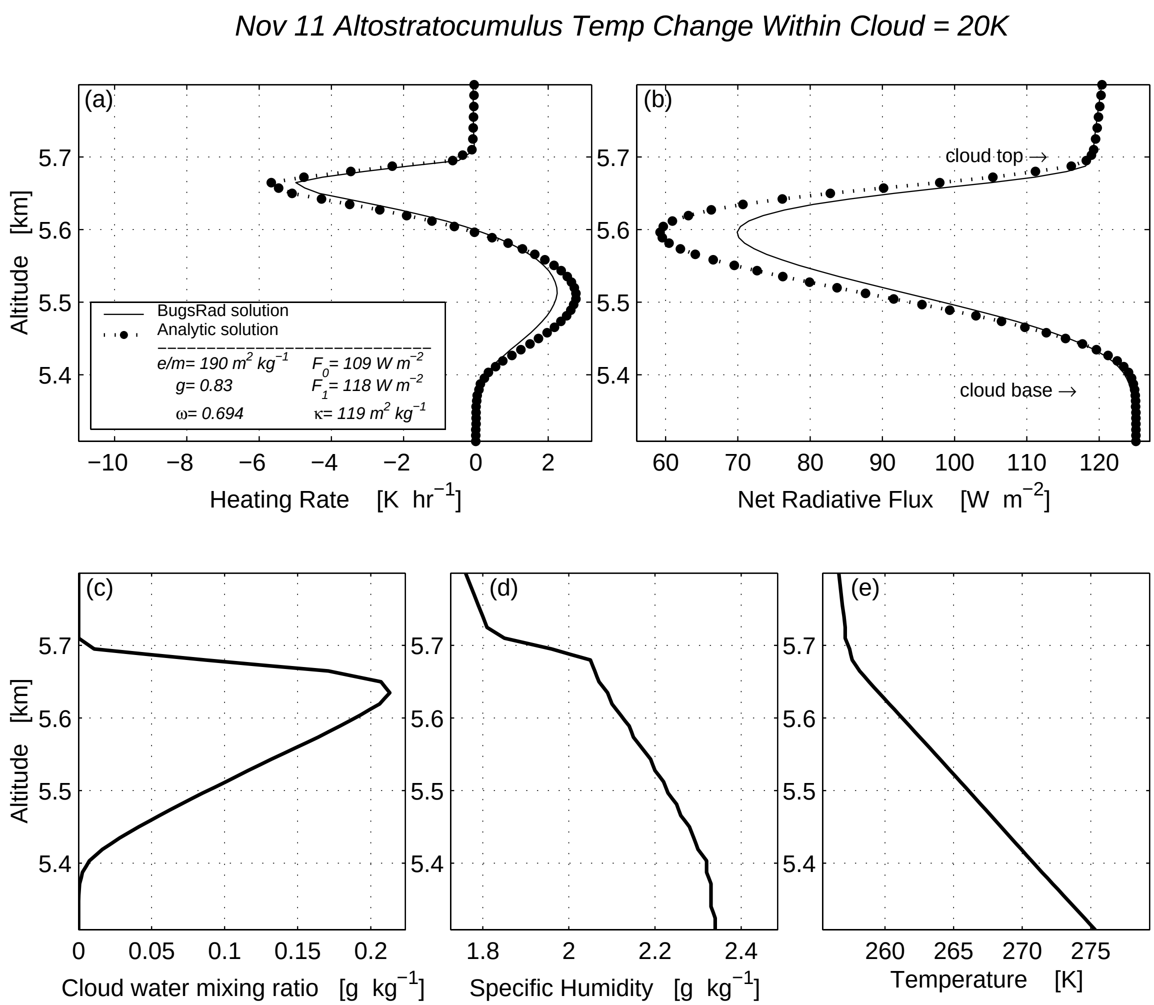

Figure 3: As in the standard case (Fig. 2), except that the within-cloud temperature differential is increased by 20 K. This violates an assumption of Eq. (14), but the errors are still acceptable.

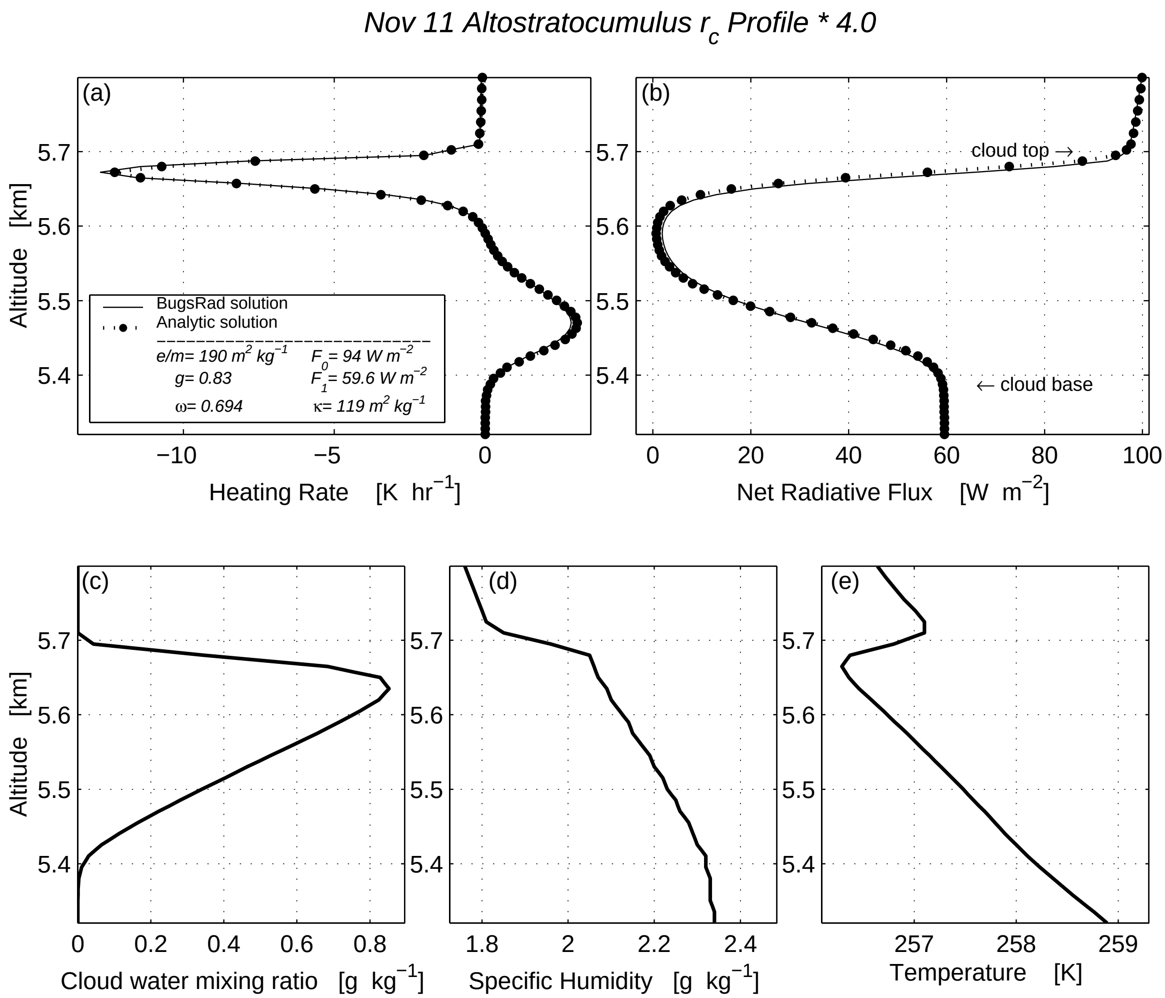

Figure 4: As in the standard case (Fig. 2), except that the cloud water mixing ratio r_c is quadrupled everywhere. The analytic solution fits the numerical solution well, with no change in the value of κ.

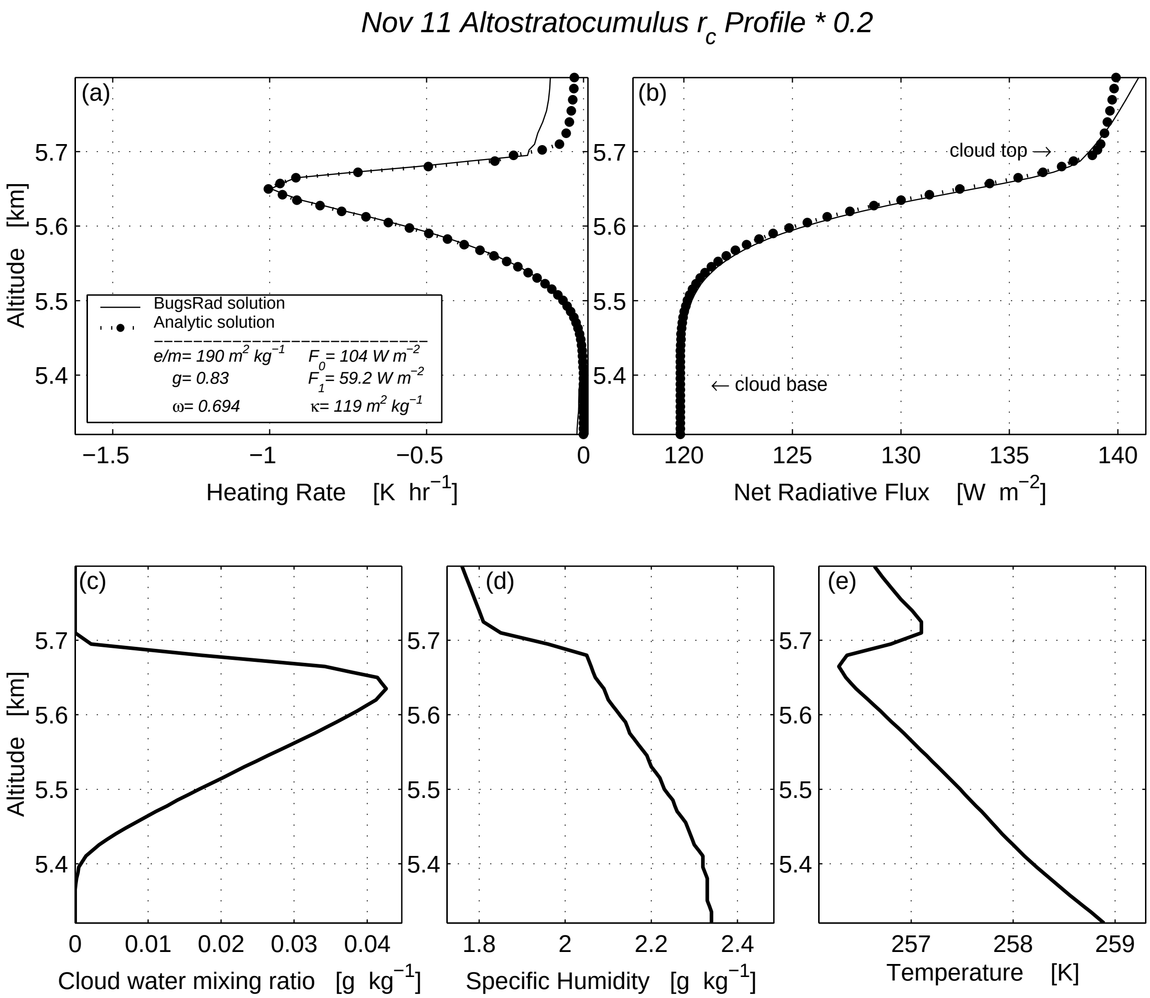

Figure 5: As in the standard case (Fig. 2), except that the cloud water mixing ratio r_c is divided by 5. The analytic solution fits the numerical solution well within cloud.

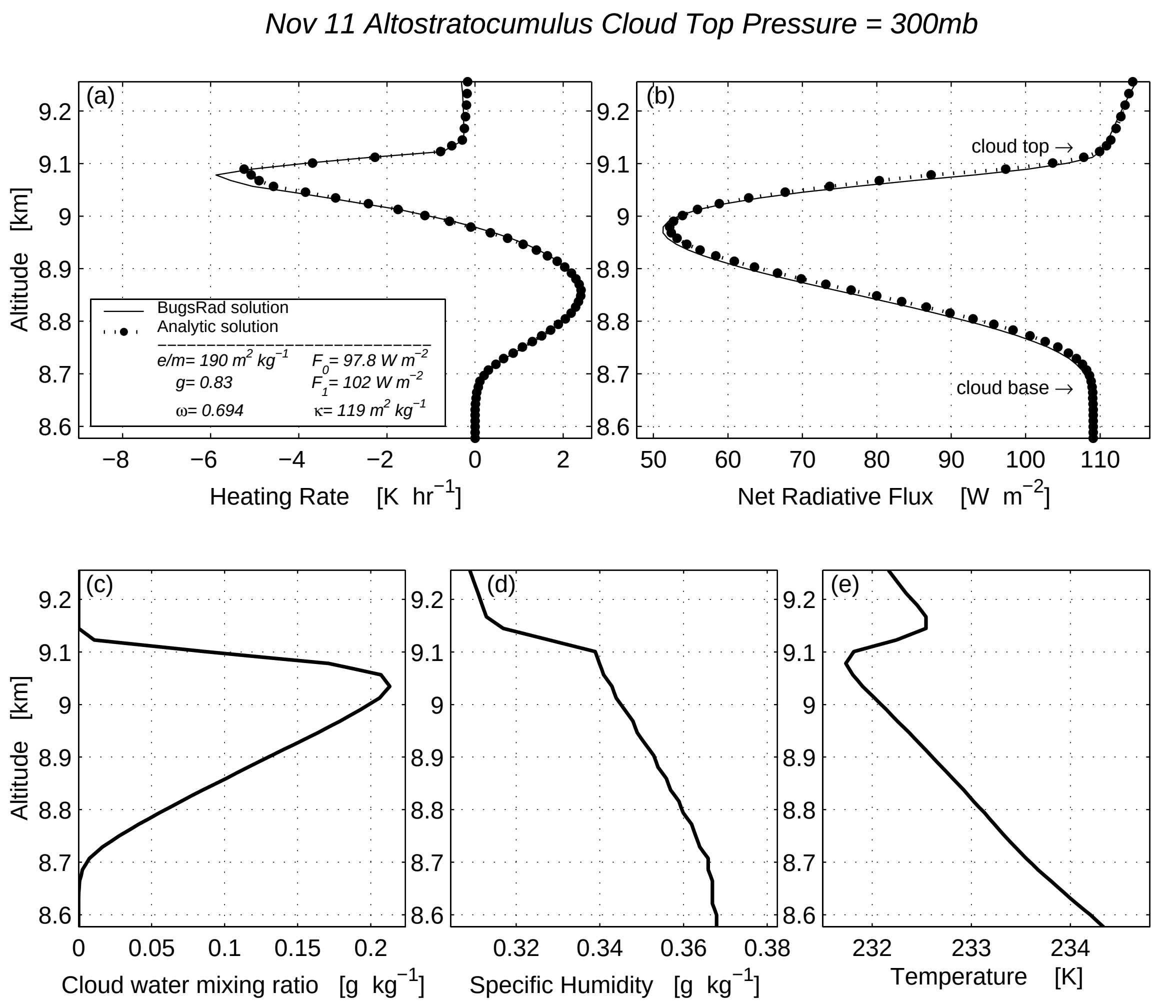

Figure 6: As in the standard case (Fig. 2), except that the cloud-top pressure has been decreased to 300 mb. The cloud base heating greatly exceeds that of the standard case (Fig. 2) because the cloud base is cooler.

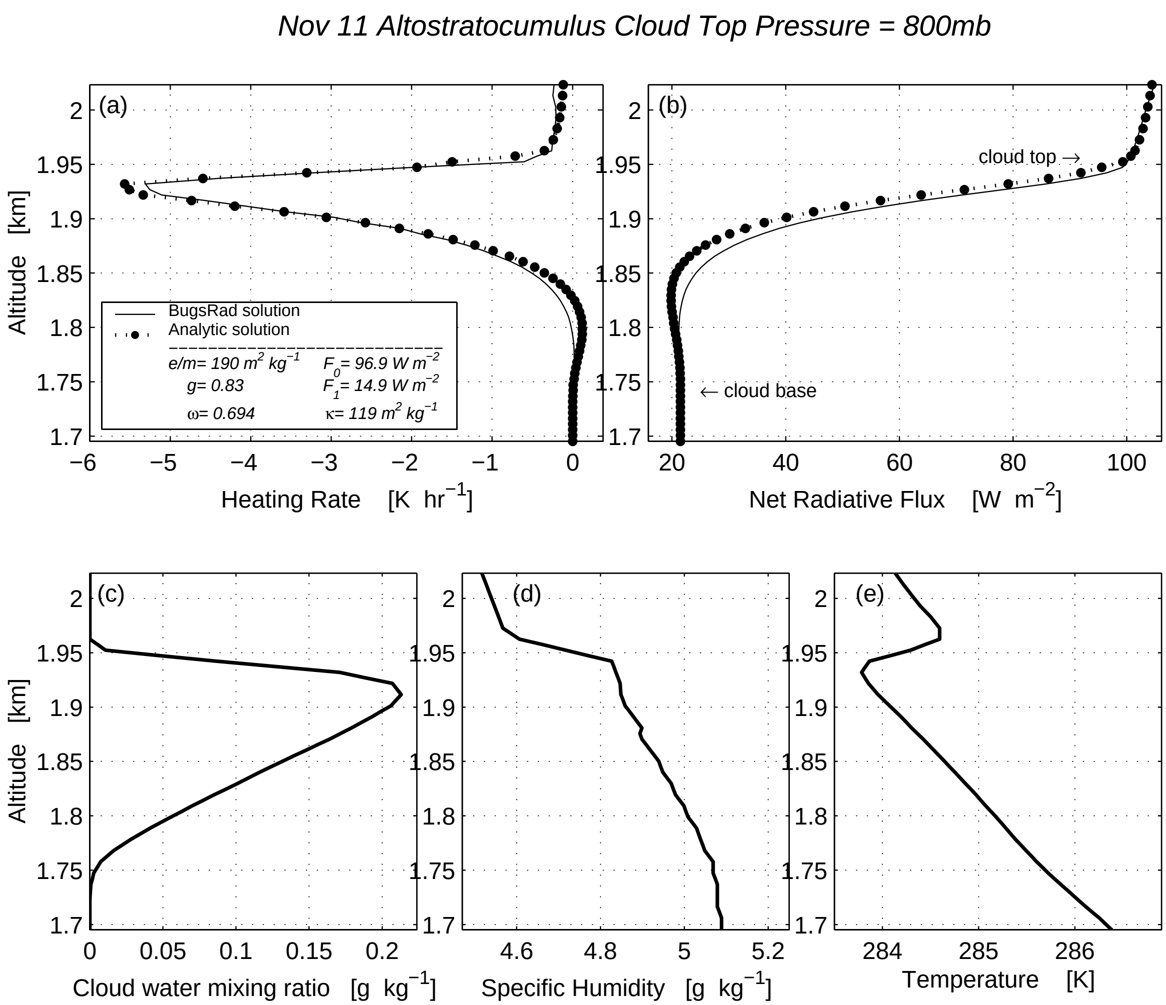

Figure 7: As in the standard case (Fig. 2), except that the cloud-top pressure has been decreased to 800 mb. The cloud base heating is now comparable to that in the DYCOMS-II RF01 boundary layer case.

Table 1: Variations of κ with effective radius r_e as computed by BugsRad. Also computed is the extinction cross-section per mass e/m (see Eq. 2), and $\alpha = \sqrt{3(1-\omega)(1-\omega g)}$ (see Eq. 1). The calculations use a liquid water content of 0.4 g m $^{-3}$ and a representative longwave radiation wavelength of 13.7 μm.

Effective radius, r_e [μm]	e/m [m^2 kg^{-1}]	α [ ]	κ [m^2 kg^{-1}]
5.0	189	1.13	213
7.5	152	1.06	160
10.0	125	1.02	127
12.5	106	0.99	105
15.0	91.2	0.98	89.5

Table 2: Best-fit parameter values of F_0, F_1, and D for the cases in our sensitivity study. All cases are altostratocumulus except the DYCOMS-II RF01 stratocumulus. We use a constant value of $\kappa = 119$ m^2 kg^{-1} rather than the best-fit κ (see Table 3), except when effective radius is changed.

Case	κ [m^2 kg^{-1}]	F_0 [W m^{-2}]	F_1 [W m^{-2}]	D [μ s^{-1}]
DYCOMS-II RF01 Sc	119	62	17.7	3.75
Standard	119	96.2	61.2	1.93
Δ T = 20 K	119	109	118	1.03
Quadrupled cloud water	119	94	59.6	2.05
0.2 $\times$ cloud water	119	104	59.2	0.58
300 mb cloud top	119	97.8	102	4.27
800 mb cloud top	119	96.9	14.9	1.85
0.4 $\times$ above-cloud vapor	119	111	60.7	1.93
0.4 $\times$ below-cloud vapor	119	96.2	69.9	1.93
5-μm effective radius	172	96.3	61.3	2.00
15-μm effective radius	89.9	96.7	61.7	1.93

Table 3: Vertically averaged root-mean-square (RMS) errors in radiative heating hate, given values of κ. Column 1 lists the case name. Column 2 lists the best-fit value of κ for each case, which is not necessarily the value of κ (usually 119 m^2 kg^{-1}) used in the figures. Column 3 lists the range of κ values that yield RMS heating rate errors of $<$ 0.5 K hr^{-1}. Column 4 lists the RMS heating rate error when the best-fit value of κ is chosen. Column 5 lists the RMS heating rate error when κ is set to the plotted values listed in Table 2 (usually 119 m^2 kg^{-1}).

Case	Best-fit κ [m^2 kg^{-1}]	Range of κ that yields RMS error $<$ 0.5 K hr^{-1} [m^2 kg^{-1}]	RMS error when $\kappa =$ best-fit value [K hr^{-1}]	RMS error when $\kappa =$ plotted value [K hr^{-1}]
DYCOMS-II RF01 Sc	100	71 - 122	0.238	0.323
Standard	119	80 - 170	0.078	0.078
Δ T = 20 K	101	74 - 131	0.129	0.329
Quadrupled cloud water	124	93 - 160	0.11	0.127
0.2 $\times$ cloud water	118	0 - 278	0.031	0.031
300 mb cloud top	126	95 - 168	0.114	0.142
800 mb cloud top	110	68 - 166	0.123	0.151
0.4 $\times$ above-cloud vapor	122	87 - 168	0.087	0.095
0.4 $\times$ below-cloud vapor	119	82 - 168	0.085	0.085
5-μm effective radius	172	120 - 240	0.146	0.146
15-μm effective radius	90	55 - 131	0.068	0.068